Assimilation of ozone profiles from the Improved Limb Atmospheric Spectrometer-II: study of Antarctic ozone

Ivanka Stajner[1,2], Krzysztof Wargan[1,2], Lang-Ping Chang[1,2], Hiroo Hayashi[1,3], Steven Pawson[1], and Hideaki Nakajima[4]

[1] Global Modeling and Assimilation Office, NASA Goddard Space Flight Center, Greenbelt, Maryland
[2] Science Applications International Corporation, Beltsville, Maryland
[3] Goddard Earth Sciences and Technology Center, University of Maryland Baltimore County, Baltimore, Maryland
[4] National Institute for Environmental Studies, Tsukuba, Japan

Abstract. Ozone data from the Improved Limb Atmospheric Spectrometer-II (ILAS-II) were included in addition to other satellite observations in the ozone assimilation system at the Global Modeling and Assimilation Office (GMAO) of NASA/Goddard. The control run assimilated data from NOAA 16 Solar Backscatter Ultraviolet/2 (SBUV/2) and Polar Ozone and Aerosol Measurement III (POAM III) instruments. Persistent impacts over Antarctica and transient impacts over northern middle and high latitudes are seen from April to October 2003, when ILAS-II provided good coverage. The largest improvements with respect to independent ozone sonde data are seen over the South Pole station. Ozone analyses and forecasts from the assimilation of SBUV/2, POAM III and ILAS-II data are used to investigate the transport of ozone to southern middle latitudes following the breakup of the Antarctic vortex. The quality of analyses and forecasts is evaluated by comparison with independent Stratospheric Aerosol and Gas Experiment III (SAGE III) ozone data near 46°S. Anomaly correlations between SAGE III data and forecasts exceed 0.6 for up to five to seven days at 30, 50, and 70 hPa. The loss of skill with advancing forecast length is related to dynamical errors due to an excessively persistent vortex in longer forecasts, which hampers the transport of low ozone air into middle latitudes.

1. Introduction

The importance of ozone to terrestrial climate and ecosystems motivates a wide range of modeling and observational initiatives that aim to further our understanding of the processes that determine the time-dependent ozone distribution. Ozone data assimilation bridges the gap between models and observations, being a powerful technique for providing optimal estimates of the global ozone distribution using state-of-the-art models to interpolate the sometimes sparse observations to poorly observed regions. Ozone assimilation systems typically incorporate retrievals of daytime ozone obtained from measurements of backscattered solar irradiance (e.g., Long et al., 1996; Stajner et al., 2001; Eskes et al., 2003; Dethof and Holm, 2004). Such measurements generally give good horizontal coverage, but rather coarse vertical resolution, so the success of the assimilation depends on the skill of the model. There is often much uncertainty in the assimilated products, especially in two regions which are important to

the environment: near the polar night, where drastic ozone loss is possible, and below the ozone maximum, which is crucially important for climate forcing. This motivates including different types of data, determined from limb-sounding emission and occultation techniques.

Solar occultation instruments provide accurate ozone profiles, with high vertical resolution (up to 1 km) down to cloud top, but these are spatially sparse with only about 15 profiles near a constant latitude in each hemisphere on any day (e.g., Randall et al., 2003; Brühl et al. 1996; Wang et al. 2002; Nakajima et al., 2005). Assimilating these data presents a unique opportunity to benefit from their vertical information content, but a significant challenge because of their low horizontal density. Occultation data have thus typically not been assimilated, but have been used as high-quality validation datasets (e.g., Stajner et al., 2001, 2004; Wargan et al., 2005). The potential value of occultation data in constraining assimilated fields in and around the Antarctic polar vortex has been demonstrated by Stajner and Wargan (2004), who demonstrated positive impacts on the polar ozone profiles when Polar Ozone and Aerosol Measurement (POAM) III retrievals were added to the Solar Backscattered Ultraviolet/2 (SBUV/2) data in the NASA Goddard ozone data assimilation system.

In the present paper we evaluate the impacts of assimilating Improved Limb Atmospheric Spectrometer-II (ILAS-II) ozone data in a similar system that already assimilates ozone data from SBUV/2 and POAM III instruments. The study is done over the Antarctic winter and spring 2003 when ILAS-II data were available. Total ozone values reached lower levels than in any of the preceding 16 years at two stations in southern middle and high latitudes: Marambio (62°S) and Ushuaia (55°S) (Pazmiño et al. 2005). Given that ILAS-II and POAM III are both occultation instruments making measurements at nearby locations we ask the following questions: (i) Is there any additional impact from including ILAS-II data to the system that already assimilates SBUV/2 and POAM III data? (ii) Does constraining ozone values in the Antarctic vortex through assimilation of POAM III and ILAS-II data help forecasting of ozone evolution in the southern middle latitudes following the vortex breakup?

2. Assimilation system

Data assimilation provides a methodology for combining information from models and observations, according to their error characteristics, in order to provide optimal estimates of spatio-temporal distribution of geophysical fields (Daley, 1991). The ozone assimilation work at NASA/Goddard (Stajner et al., 2001) uses the sequential Physical-space Statistical Analysis System (Cohn et al., 1998).

The version of ozone assimilation system used here is based on that described by (Stajner et al., 2004) with the following enhancements. The ozone transport is implemented within the Goddard Earth Observing System Version 4 (GEOS-4) general circulation model (GCM). The stratospheric gas-phase chemistry parameterization is based on the work of Douglass et al. (1996), with adjustments to ozone production rates in the upper stratosphere to reproduce an ozone climatology (cf. Stajner et al., 2004). The ozone assimilation remained univariate, and possible feedbacks of ozone into radiative calculations or infrared radiance assimilation were not used. All the meteorological variables other than ozone (e.g. temperature and winds) are

taken from the Global Modeling and Assimilation Office (GMAO) operational analyses with the GEOS-4 system: GEOS-4.0.2 version from January to mid May, followed by its GEOS-4.0.3 version to the end of the study period (Bloom et al., 2005). The GCM includes flux-form semi-Lagrangian transport (Lin and Rood 1996) at 1.25° longitude by 1° latitude resolution and 55 eta-levels between the surface and 0.01 hPa.

3. Ozone data

In this study NOAA 16 SBUV/2 Version 6 retrievals of total ozone columns and partial ozone columns in 5 km thick layers at pressures less than 64 hPa (Umkehr layers 4 to 12) are used (Bhartia et al. 1996). The nadir sounding geometry of the SBUV/2 instrument and the choice of measured wavelengths pose constraints on the vertical resolution of ozone retrievals. The physical principle of measurements of backscattered solar radiation limits the coverage to sunlit part of the globe, leaving polar night regions unobserved. Observation error specifications used in this study are taken from Stajner et al. (2001) for stratospheric partial columns and the standard deviations for the total columns are 2.5%.

The ILAS-II instrument provided ozone profiles from solar occultation measurements in year 2003, with the best coverage from April to October (Nakajima et al., 2005). ILAS-II Version 1.4 ozone profiles used in this study were validated by comparisons with ozone sondes and other satellite sensors: Halogen Occultation Experiment (HALOE), POAM III, Stratospheric Aerosol and Gas Experiment (SAGE) II and SAGE III (Sugita at al., 2005). On each day at most 15 ILAS-II profiles are retrieved in each hemisphere at nearly constant latitudes. Despite their sparseness the ILAS-II profiles are complementary to SBUV/2 because of their better vertical resolution and poleward coverage during southern winter and spring. All ILAS-II ozone data were assimilated, typically between the pressures of about 130 and 0.3 hPa, using random errors provided in the data files as observation errors.

The POAM III instrument provides solar occultation profiles at almost identical latitudes as ILAS-II. Because of problems with the instrument during year 2003 the measurements were taken in only one hemisphere on each day, alternating between north and south on consecutive days. Following Stajner and Wargan (2004) we assimilated POAM III data between 14 and 60 km using specified observation errors of 5%. Most of the results in this study use Version 3 of POAM III data (Lumpe et al., 2002; Randall et al., 2003). Recently released Version 4 of POAM III retrievals includes improved instrument pointing and altitude determination (J. Lumpe, personal communication, 2005). These data were used to help interpret the differences that were found between ILAS-II data and Version 3 of POAM III data.

Two sources of independent data are used for validation of results in this study: the South Pole ozone sondes (Hofmann et al., 1997) and SAGE III ozone profiles (Taha et al., 2004), which both provide high quality, vertically resolved data in the lower and middle stratosphere. The South Pole station is typically within the core of the polar vortex, where substantial impacts are expected in the assimilation of ILAS-II and POAM III data. Following the breakup of the polar vortex we want to investigate the impact of ozone-depleted air on southern middle latitudes, which are observed by SAGE III occultation profiles at sunrise.

4. Impacts of ILAS-II data

The impacts of adding ILAS-II data to the assimilation that already uses SBUV/2 and POAM III data are shown in Fig. 1. In the lower stratosphere at 70 hPa, the use of ILAS-II data increases ozone values in the core region of the polar vortex. The impact increases with time from ~2% in May, to ~5% in July, and finally to ~10% in September. Note the distinction between increased ozone in the vortex core region versus a slight decrease in the ozone towards the vortex boundary in September. The distinction between mixing properties of these two regions was pointed out by Lee *et al.* (2001). In the middle stratosphere at 30 hPa, the assimilation of ILAS-II data reduces ozone over Antarctica. The largest impact of ~20% is seen in May, and it diminishes with time to ~10% in July and further to ~5% in September. The relative errors of ILAS-II data in the lower stratosphere increase with decreasing ozone values in September and October, and thus the impact of ILAS-II data on the assimilated ozone is reduced in October.

The ILAS-II data have a smaller impact in the summertime northern hemisphere that rarely exceeds 5%. The smaller impact is consistent with the larger relative errors reported for ILAS-II data there. Furthermore, different meteorological conditions between the two hemispheres lead to vastly different situations for these sparse data types. In the Antarctic, many of the occultation observations are located inside the polar vortex, which is dynamically isolated from the middle latitudes. This allows the impact of the ILAS-II data to build up coherently inside the vortex, where there are no other observations to constrain the ozone distribution. In the northern hemisphere, two effects are important. First, at and above the ozone maximum, the constraint by the accurate SBUV/2 data means that the ILAS-II data have a much smaller impact than in the polar night. Second, the absence of a mixing barrier in the summer means that air masses in the lower stratosphere that are subject to ILAS-II constraints are rapidly transported through middle and high latitudes and not persistently constrained as in the Antarctic. This highlights that the occultation data are most useful when applied repeatedly to the same subset of air masses, as occurs in the isolated polar vortex throughout the winter.

The largest impact of ILAS-II data is seen near the South Pole, whether ILAS-II measurements were close to it as in September or further away as in July. Independent ozone sonde profiles at the South Pole are used in evaluation of the quality of assimilation runs (Fig. 2). On July 10 the assimilation that used SBUV/2 and POAM III data overestimates the ozone between 20 and 50 hPa and underestimates the ozone between 70 and 150 hPa. The assimilation that includes additional data from the ILAS-II instrument typically has lower ozone values around 30 hPa and higher ozone values near 70 hPa. Both of these changes improve the agreement between the assimilated ozone and the ozone sonde profile. Similar impacts were seen in most comparisons with the ozone sondes at the South Pole in June and July. In October the assimilation of SBUV/2 and POAM III data already agrees well with the ozone sonde profile, and the addition of ILAS-II data has a very small impact. As expected, the addition of POAM III and ILAS-II occultation data to the assimilation that uses only SBUV/2 (not shown) improves Antarctic ozone profiles in winter and spring, resembling the enhancements seen from assimilation of POAM III data by Stajner and Wargan (2004).

Specific impacts of ILAS-II data can be attributed to differences between ILAS-II and POAM III instrument coverage, error specifications that were used in the assimilation of their

data, and to the retrieved ozone values. During the period studied here the POAM III instrument experienced difficulties in regular operation. Instead of observing both hemispheres on each day, POAM III made measurements in only one hemisphere on each day, alternating between north and south. Consequently, the amount of POAM III data is about a half of those that were available in 1998 and used by Stajner and Wargan (2004). Following their work, we used Version 3 retrievals of POAM III ozone with observation errors of 5% in the assimilation experiments. Error estimates included in the ILAS-II data files were used in the assimilation of ILAS-II data in order to help in validation of not only ILAS-II ozone, but also of the error estimates. There is a strong time dependence in the relative error estimates for ILAS-II ozone. At 70 hPa they increase from about 15% for the period between April and September (Fig. 3a) to more than 50% in October (Fig. 3b). Consequently the impact of ILAS-II data diminishes in October, but a substantial improvement was seen at the South Pole in July (recall Fig. 2). The improved profile shape could be due to the use of additional ILAS-II data with relatively low errors. However, the shape of ILAS-II and POAM III profiles differ as well (Fig. 4b). On average, compared to either version of POAM III retrievals, ILAS-II provides lower ozone between 10 and 40 hPa, and higher ozone between 50 and 100 hPa in the beginning of July. This is consistent with the impact seen from ILAS-II data in July (Fig. 2). Note that in April profiles from Version 4 of POAM III retrievals agree more closely with ILAS-II profiles than those from Version 3 of POAM III retrievals (Fig. 4a). The improvements in the assimilated ozone in July over the South Pole are due not only to the use of additional ILAS-II data with good coverage and relatively small error specifications, but also to the ILAS-II profile shape that differs from that of Version 3 of POAM III data. Based on the size of the differences between ILAS-II and Version 4 of POAM III profiles (Figs. 4a, 4b) we expect that when Version 4 POAM III data are used in the assimilation the impact of adding ILAS-II will be smaller on May 1 compared to Fig 1b, but that the impact on July 10 will be comparable to that shown in Figs. 1c, 1d.

5. Ozone evolution over Antarctica

Monthly mean fields from SBUV, POAM III and ILAS-II assimilation describe qualitatively the evolution of lower stratospheric temperature and ozone during Antarctic spring. Mean fields for September are shown in the top row of Fig. 5. The Antarctic vortex (marked by lowest temperatures) shows a hint of the zonal wave number three. Recall that wave number three was seen in the shape of the vortex on September 15 (Fig. 1e). There is also a shift of the vortex towards 45°W, which induces zonal wave number one in temperature and ozone fields. The ozone depletion that starts at the vortex edge does not fully advance towards the South Pole in the September average yielding ring-like shape of the lowest ozone. Model tendencies attempt to make the ozone field more zonal by increasing ozone east of the dateline and decreasing ozone east of the Greenwich meridian. In contrast, the analysis increments of the opposite sign are trying to strengthen zonal asymmetry in ozone. The average temperature field in October (Fig. 5, bottom row) shows that the vortex is shifted towards 45°E. Ozone within the vortex is fully depleted. The analysis increments are similar to those seen in September. However, the model tendencies are dominated by the dynamical events at the end of October. The elongation of the vortex at the end of October roughly in the direction of the 60°E-240°E and the squeezing of the vortex in the orthogonal direction causes the largest positive model

tendencies. Ozone rich air from outside the vortex displaces ozone-depleted air from within the vortex (see positive model tendencies near 150°E).

This example shows how assimilation of sparse occultation data helps to provide a coherent picture of the ozone evolution in the Antarctic polar stratosphere. The assimilating model supplies accompanying temperature fields, dynamical and chemical tendencies. Together with data induced analysis increments they provide a comprehensive description of the ozone evolution during winter and spring.

6. Ozone forecasts in springtime

The elongation of the vortex that started in late October intensifies in November, leading to vortex breakup and transport of ozone-depleted air from the vortex core into southern middle latitudes. This process is illustrated by a series ozone analyses (Fig. 6). At 30 hPa, ozone-depleted air crosses 45°S near 60°E on November 1, after when it is advected eastward before separating from the remainder of the vortex before November 9 (top row). At 70 hPa the low ozone air that is at 45°S near 90°E on November 1 is advected eastward and returns poleward, where it can be seen near 225°E on November 9 (bottom row). Note a distinct zonal wave number three pattern in the ozone field on that day. The ozone low that was near 300°E on November 5 is advected towards middle latitudes and reaches 45°S near the dateline on November 9. (Behavior at 50 hPa is similar to that at 70 hPa.)

The vertical structure of the elongated ozone feature is illustrated by a longitude-pressure section at 50°S on November 5 (Fig. 7). This reveals an eastward slope (with increasing altitude) of the low ozone feature, with the corresponding higher ozone values from outside the polar vortex on its eastern flank. Temperature contours illustrate the correspondence of this ozone feature with the occurrence of a baroclinic zone. This is dynamically similar to those examined during warming events in the 1984-1985 northern winter by Fairlie et al. (1990). Figure 7 shows that the baroclinic feature is quite deep, extending between about 70 hPa and 20 hPa. This complex dynamics together with high gradients in ozone that were set up by previous chemical processes make early November an interesting period for a study of the evolution of ozone in southern middle latitudes.

During early November, SAGE III is making measurements near 46°S. In order to evaluate the realism of the ozone analyses and forecasts, they are compared with SAGE III data. SAGE III data are binned to the nearest 10° longitude and plotted using colored squares over the underlying analysis or forecast field, using an identical color scale (Fig. 8). The most prominent feature in the time series at 30 hPa is the low ozone starting near 60°E on November 1, with an accompanying high ozone near 90°E (Fig. 8a). This feature travels eastward as it diminishes in strength, disappearing by around November 10. SAGE III measurements near this feature confirm the realism of both low and high ozone values and their eastward propagation. Note that away from this feature the ambient midlatitudinal air has not been constrained by ILAS-II or POAM III data, but only by SBUV/2 data, and that it is on average lower than the SAGE III values. The comparison of SAGE III with the forecast that was started on October 30 at 18z shows similarly good agreement, with somewhat less low-ozone air

passing through around November 5 (Fig. 8b) and a hint of a reduced ozone bias in the ambient midlatitudinal air.

At 70 hPa the agreement between SAGE III and analyses in the depth and the breadth of the low ozone around 90°E on November 3 (Fig. 8c) is quite good. The regions with depleted ozone are transported realistically in the analyses. However, there are some clear discrepancies in the ozone forecast (Fig. 8d). The low ozone feature in the forecast seen near 60°E on November 8 advanced too far east in comparison with both analyses and SAGE III data. Note also the ozone low passing near the dateline in the analyses on November 14, which agrees well with the SAGE III data (Fig. 8c). Qualitative comparison of features in the analyses and forecasts with SAGE III ozone shows that they are captured quite realistically, with indication of some biases in the analyses and with excessive eastward propagation due to the dynamical developments in the forecasts.

A quantitative measure of the forecast quality is provided by anomaly correlations, which are commonly used for forecast verification in the numerical weather prediction (NWP) (e.g., Wilks 1995). A time series of the differences between all SAGE III data at each level for November 1-10 and their mean was constructed. Another time series of the differences between model fields (at SAGE III locations) and their mean was constructed. A correlation between these time series was computed for model fields as a function of the forecast length, where analyzed fields are used for length zero. The time series of anomaly correlations at 70 and 30 hPa are shown in Fig. 9. Note that independent SAGE III data were used for verification, meaning that the anomaly correlations for the analyses (day zero) are less than one. In traditional NWP usage, anomaly correlations start at unity for forecast length zero, because forecasts are verified against the analyses. The value at day zero in these calculations gives a measure of disagreement between the analyses and the independent SAGE III data. At 70 hPa the anomaly correlations exceed 0.9 for two days, remain above 0.8 for four more days, and fall below 0.6 on day seven. At 30 hPa there is an initial increase in the anomaly correlations from 0.8 for analyses to 0.88 for the three-day forecasts. The analyses of the ambient midlatitudinal air tend to be too low compared to SAGE III values. Within the first three days the forecasts drift away from the analyses, increasing the mean field, bringing it closer to SAGE III mean, and improving the baseline for computation of anomaly correlations. On day 6 the anomaly correlations fall below 0.6. The nonmonotonicity of anomaly correlations with time is likely due to a small sample size and to an initial bias in the analyses at 30 hPa. A study spanning several winters is needed to examine how robust these results are. Nevertheless, we found useful forecast skill (anomaly correlation exceeding 0.6) for 5-6 days at 30, 50 and 70 hPa in southern middle latitudes following the vortex breakup in November 2003 using SAGE III data for verification.

Representation of constituent data using their probability distribution function (PDF) provides another view of the data that may help in characterizing their basic statistical properties, as well as contributions of different transport regimes (e.g., Sparling 2000). The PDFs for all the SAGE III sunrise data in 0.33-ppmv-wide bins for November 1-10 at 70 or 30 hPa are shown in Fig. 10. They are compared with PDFs of all model data at 46°S at the same level during November 1-10. Note that data from all 288 model grid points 1.25° longitude apart at all four synoptic times per day are used. Three instances of the model fields are used:

analyses, five-day forecasts and seven-day forecasts. At 70 hPa SAGE III data have a stronger mode at 2 ppmv than the analyses (Fig. 9a). With an advancing forecast length the mode becomes more pronounced at the expense of under-representing lower (1.3 ppmv) or higher (2.66 ppmv) values. Both analyses and forecasts have too many points in the 2.3 ppmv bin compared to SAGE III.

At 30 hPa SAGE III data show three peaks in the distribution (Fig. 9b). Most of the air has midlatitudinal values (close to the mode at 5.33 ppmv). Lower values around 3.66 ppmv are suggestive of air that was previously within the vortex core. A possible pathway for the air with higher values around 6.66 ppmv is that it originated in the tropics, traveled poleward, possibly even descending near the vortex edge, then being advected back into middle latitudes during vortex breakup. In the analyses, the mode is shifted a bin lower than in SAGE III, indicating the low bias in the analyses. Forecasts have an increasingly stronger mode with advancing forecast length, meaning the ozone field becomes more uniform as the forecasts advance, possibly due to stronger barriers to meridional transport. The seven-day forecasts do not capture the very low ozone values of 2.6 ppmv, which are represented in the analyses and five-day forecasts. Note that the spatial sampling of SAGE III poses limitations for interpretation of the low ozone air that is crossing 46°S around 60°E on November 1 (Fig. 8a). In the analyses this feature spans only about 30° of longitude and SAGE III measures near its edges, never quite seeing the region where the analyses have their lowest values. The largest difference between the PDFs for the three-day forecast (not shown) and the analyses is the shift of values from the 4.66- to the 5-ppmv bins, which increases the mean of the forecast and brings it closer to SAGE III. This supports the possible explanation of the increase in the anomaly correlations due to the bias reduction that was mentioned in the discussion of Fig. 9.

Some of the loss in the forecast skill is manifested as spatial misalignment between the low or high ozone features in the forecast flow and verification data. For example, a five-day forecast for November 5 at 30 hPa is shown in Fig. 11a. Compared to the ozone analysis at the same time (Fig. 6, top center panel), the forecast field suggests an excessively barotropic, solid-body like rotation. More pronounced symmetry in the forecast than in the analyzed ozone is consistent with an average zonal wind that is more than 5 m/s stronger in the forecasts than in the analyses near 30 hPa and 75°S (Fig. 11b), and with fewer low ozone values in the middle latitudes due to a stronger mixing barrier at high latitudes (Fig. 10b).

7. Conclusions

This study uses solar occultation data from two instruments, ILAS-II and POAM III, together with data from the nadir-viewing NOAA 16 SBUV/2 instrument within a global ozone assimilation system. Substantial impacts of ILAS-II data are found within the Antarctic vortex in the year 2003 (Fig. 1). The use of ILAS-II data improves the comparison of ozone analyses with the South Pole ozone sonde in the winter (Fig. 2). A study of ozone evolution in the southern middle latitudes following the breakup of the Antarctic vortex reveals realistic representation of ozone variability in the analyses (Figs. 6-7). This is followed by qualitative and quantitative comparisons of analyses and forecasts against independent SAGE III data near 46°S (Figs. 8-10). Anomaly correlations exceed 0.6 for up to 5-7 days in the middle and lower stratosphere (30, 50 and 70 hPa). The loss in the forecast skill with advanced forecast length

seems to be related to a stronger zonal wind (Fig. 11b) that could pose a barrier to transport of low ozone air to middle latitudes (Fig. 10b) and possibly also cause an eastward shift in flow features (Fig. 11a).

The evolution of ozone at two levels is investigated. At 70 hPa there is a large dynamic range of values due to an ozone accumulation in wintertime, and a full depletion in the spring inside the "ozone hole". At 30 hPa near the top of the "ozone hole" the ozone loss is more subtle (Fig. 2). With respect to Version 3 retrievals from POAM III instrument that were used in most of this study, ILAS-II ozone is typically lower than POAM III ozone at 30 hPa, and ILAS-II ozone is typically higher than POAM III ozone at 70 hPa in the southern hemisphere between April and August. Version 4 of POAM III retrievals accounts for pointing problems of the instrument, bringing these data to closer agreement with ILAS-II, but not uniformly in time. We expect that the impact of using ILAS-II data will change when Version 4 of POAM III data is used in a time dependent fashion. Based on the comparisons of raw data (Fig. 4), the impact of ILAS-II is expected to decrease in April, but remain comparable to those seen in Figs. 1 and 2 in July.

The evolution of low ozone air masses is of interest for estimation of surface UV radiation (Pazmiño et al. 2005). Assimilation of occultation data into an ozone model provides a way of estimating ozone within the vortex, and the forecasting capability provides a way of predicting the evolution of the low ozone air as it enters middle latitudes in the springtime. The value of occultation data for surface UV forecasts over South America using assimilation of ozone data into a three-dimensional model could be evaluated in a future study.

The analyses successfully propagate the information from the Antarctic vortex into middle latitudes in November. The forecast are relatively successful in predicting ozone variability, but show somewhat excessive eastward transport and vortex persistence, which also poses a barrier to transport of air away from the pole. The dynamical nature of errors in the ozone forecasts raises another possibility. If occultation data were available even a day or two after measurements were taken, they could be assimilated into a three-dimensional model to provide an initial condition with a realistic representation of the Antarctic vortex. The model could be then integrated using analyzed meteorological fields up to the real time. The use of analyzed meteorology would allow more accurate representation of the dynamics during this past period. A day or two long forecast issued from the present time would likely still contain the information from previous occultation data and would not suffer from the accumulation of dynamical errors seen in the longer forecasts. We plan to investigate this option in the future.

The use of occultation data is critical for the success of this study. When only SBUV/2 data are assimilated ozone depletion at 70 hPa inside the vortex is not fully captured. Consequently the transport of that air to middle latitudes does not decrease the ozone to the values seen by the SAGE III instrument. This demonstrates the value for assimilation of data from space based occultation instruments such as POAM III and ILAS-II, whose orbits facilitate repeated observations within the Antarctic vortex. The assimilation of such occultation data improves the qualitative and quantitative agreement with independent measurements (from sondes and SAGE III) and provides opportunities for the further study of the impacts of ozone-depleted vortex air on the southern middle latitudes in springtime. It is planned to compare the impacts

of these occultation data with those of limb-emission data (e.g., MIPAS assimilation: Wargan et al., 2005), which have the advantage of better spatial coverage but generally have less vertical resolution and lower precision. A potential advantage of occultation data is that the unified record of such observations spans several years, compared to the shorter periods observed with limb-emission measurements, making them better suited for study of interannual variations in polar ozone and its dispersion into middle latitudes.

Acknowledgments

References

Bhartia, P. K., R. D. McPeters, C. L. Mateer, L. E. Flynn, and C. Wellemeyer (1996), Algorithm for the estimation of vertical ozone profile from the backscattered ultraviolet (BUV) technique. *J. Geophys. Res.*, 101, 18793-18806.

Bloom, S. C. et al. (2005), The Goddard Earth Observing System Data Assimilation System, GEOS DAS Version 4.0.3: Documentation and Validation, *Technical Report Series on Global Modeling and Data Assimilation 104606*, 26, NASA, Goddard Space Flight Center, Greenbelt, Maryland, pp. 181.

Brühl, C. et al. (1996) HALOE Ozone Channel Validation, *J. Geophys. Res.*, 101, 10,217-10,240.

Cohn, S. E., A. da Silva, J. Guo, M. Sienkiewicz, D. Lamich (1998), Assessing the Effects of Data Selection with the DAO Physical-Space Statistical Analysis System, *Mon. Wea. Rev.*, 126, 2913-2926.

Daley, R. (1991), *Atmospheric Data Analysis*, Cambridge University Press, Cambridge.

Dethof, A, and E. V. Hólm (2004), Ozone assimilation in the ERA-40 reanalysis project, *Q. J. R. Meteorol.Soc.*, 130, 2851-2872.

Douglass, A., C. Weaver, R. Rood, and L. Coy (1996), A three-dimensional simulation of the ozone annual cycle using winds from a data assimilation system, *J. Geophys. Res.*, 101(D1), 1463–1474.

Eskes, H. J., P. F. J. van Velthoven, P. J. M. Valks, and H. M. Kelder (2003) Assimilation of GOME total ozone satellite observations in a three-dimensional tracer transport model, *Q. J. R. Meteorol. Soc.*, 129, 1663-1681.

Fairlie, T. D. A., M. Fisher, and A. O'Neill, The development of narrow baroclinic zones and other small-scale structure during simulated major warmings, Q. J. R. Meteorol. Soc., 116, 287–315, 1990.

Hofmann, D. J., S. J. Oltmans, J. M. Harris, B. J. Johnson, and J. A. Lathrop (1997), Ten years of ozonesonde measurements at the south pole: implications for recovery of springtime Antarctic ozone, *J. Geophys. Res.*, 102(D7), 8931–8944.

Lee, A., H. Roscoe, A. Jones, P. Haynes, E. Shuckburgh, M. Morrey, and H. Pumphrey (2001), The impact of the mixing properties within the Antarctic stratospheric vortex on ozone loss in spring, *J. Geophys. Res.*, 106(D3), 3203–3212.

Lin, S.-J. and R. B. Rood (1996), Multidimensionsl Flux-Form Semi-Langrangian Transport Schemes, *Mon, Wea. Rev.*, 124, 2046-2070.

Long, C. S., A. J. Miller, H. T. Lee, J. D. Wild, R. C. Przywarty, and D. Hufford (1996), Ultraviolet index forecasts issued by the National Weather Service, Bull. Amer. Meteor. Soc., 77, 729-.

Lumpe, J. D., R. M. Bevilacqua, K. W. Hoppel, and C. E. Randall (2002), POAM III retrieval algorithm and error analysis, *J. Geophys. Res.*, 107, 4575, 10.1029/2002JD002137.

Nakajima, H. et al. (2005), Characteristics and performance of the Improved Limb Atmospheric Spectrometer-II (ILAS-II) onboard the ADEOS-II satellite, *J. Geophys. Res., submitted.*

Pazmiño, A. F., S. Godin-Beekmann, M. Ginzburg, S. Bekki, A. Hauchecorne, R. D. Piacentini, and E. J. Quel (2005), Impact of Antarctic polar vortex occurrences on total ozone and UVB radiation at southern Argentinean and Antarctic stations during 1997–2003 period, *J. Geophys. Res.*, 110, D03103, doi:10.1029/2004JD005304.

Randall, C. E., et al. (2003), Validation of POAM III ozone: Comparisons with ozonesonde and satellite data, *J. Geophys. Res.*, 108(D12), 4367, doi:10.1029/2002JD002944.

Sugita, T., et al. (2005), Ozone profiles in the high-latitude stratosphere and lower mesosphere measured by the Improved Limb Atmospheric Spectrometer (ILAS)-II: Comparison with other satellite sensors and ozonesondes, *J. Geophys. Res., submitted.*

Sparling, L. C. (2000), Statistical perspectives on stratospheric transport, *Rev. Geophys.*, 38(3), 417–436.

Stajner, I., and K. Wargan (2004), Antarctic stratospheric ozone from the assimilation of occultation data, *Geophys. Res. Lett.*, 31, L18108, doi:10.1029/2004GL020846

Stajner, I., L. P. Riishøjgaard, and R. B. Rood (2001), The GEOS ozone data assimilation system: specification of error statistics, *Q. J. R. Meteorol.Soc.*, 127, 1069-1094.

Stajner, I., N. Winslow, R. B. Rood, S. Pawson (2004), Monitoring of observation errors in the assimilation of satellite ozone data, *J. Geophys. Res.*, Vol. 109, No. D6, D06309 doi:10.1029/2003JD004118.

Taha G., L. W. Thomason, C. R. Trepte, and W. P. Chu (2004), Validation of SAGE III Data Products Version 3.0, *Proceedings of the XX Quadrennial Ozone Symposium*, The International Ozone Commission, Athens, Greece.

Wang, H. J., D. M. Cunnold, L. W. Thomason, J. M. Zawodny, and G. E. Bodeker (2002), Assessment of SAGE version 6.1 ozone data quality, *J. Geophys. Res.*, 107(D23), 4691, doi:10.1029/2002JD002418.

Wargan, K, I. Stajner, S. Pawson, R.B. Rood, and W.-W. Tan (2005) Monitoring and Assimilation of Ozone Data from the Michelson Interferometer for Passive Atmospheric Sounding. *Q. J. Roy. Met. Soc., accepted.*

Wilks, D.S. (1995), *Statistical Methods in the Atmospheric Sciences. An Introduction.* Academic Press, San Diego, 467 pp.

L.-P. Chang, H. Hayashi, S. Pawson, I. Stajner and K. Wargan, Global modeling and Assimilation Office, Code 610.1, NASA Goddard Space Flight Center, Greenbelt, Maryland 20771. (e-mail: lpchang, hhayashi, spawson, istajner, or kwargan@gmao.gsfc.nasa.gov)
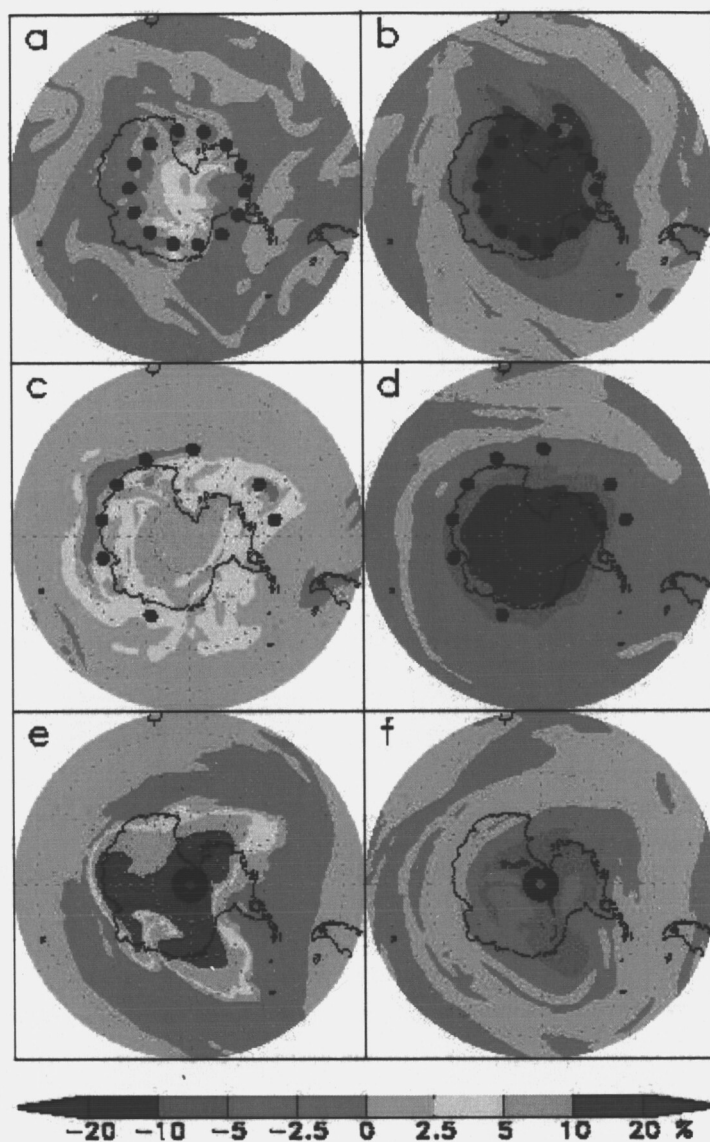
Figures

Figure 1. Maps of percentage differences between assimilation of SBUV/2, POAM III and ILAS-II data (SPI) and assimilation of SBUV/2 and POAM III data (SP). The percentage difference SPI-minus-SP is shown at 70 hPa (a, c, e) and 30 hPa (b, d, f) on three days: May 1 (a, b), July 10 (c, d) and September 15 (e,f). Southern polar stereographic maps up to 45°S are used and the locations of ILAS-II data are marked by black circles.
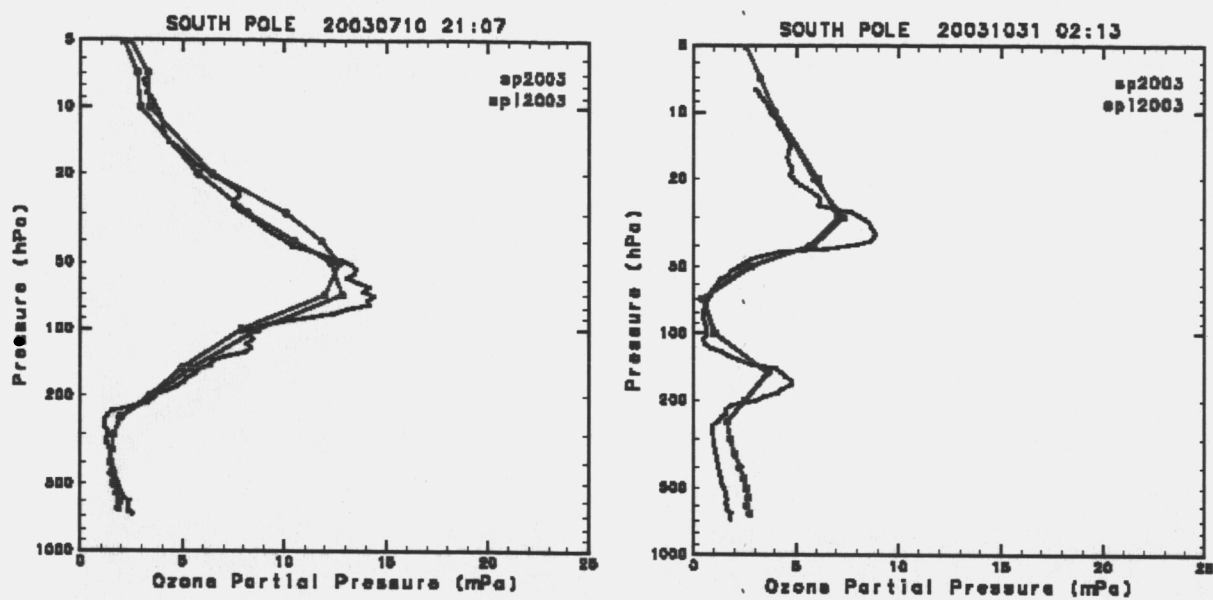
Figure 2. Comparisons of ozone sonde profiles at the South Pole (black) on July 10, 2003 (left) and October 31, 2003 (right) with collocated profiles from SP analyses (red) and SPI analyses (blue).
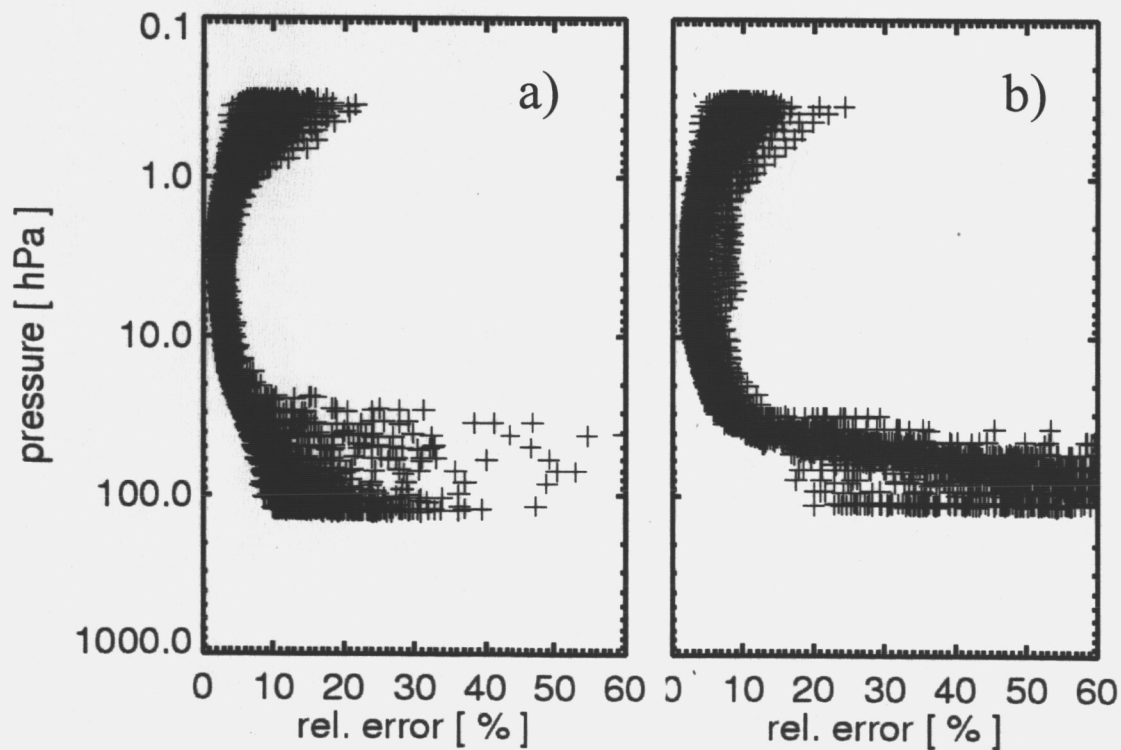
Figure 3. ILAS-II error estimates for all the profiles in the southern hemisphere in a) June and b) October 2003.

a)   b)
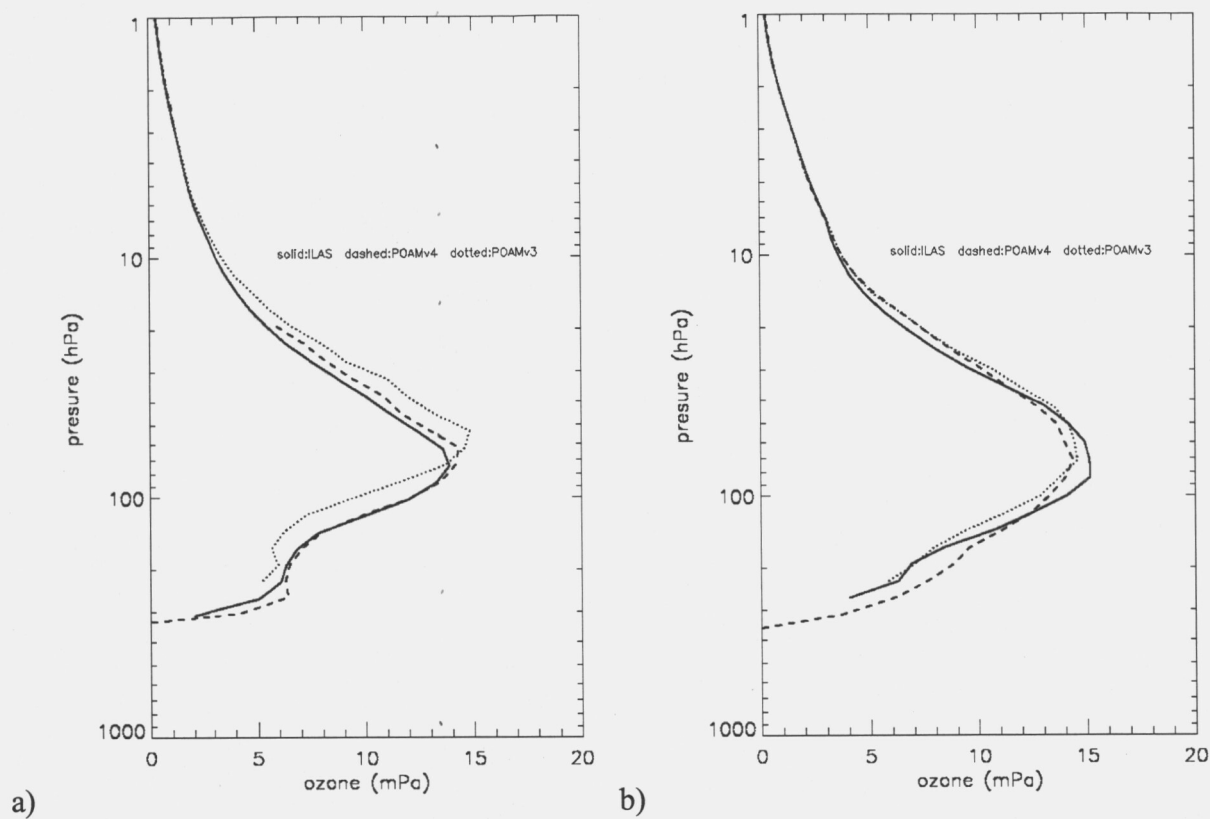
Figure 4. Mean of the profiles at the southern hemisphere of ILAS-II ozone (solid), POAM III Version 3 ozone (dotted) and POAM III Version 4 ozone (dashed). The POAM III measurements were alternating between northern and southern hemisphere on consecutive days. Averages for five days are shown: a) April 23, 25, 27, 29, May 1 and b) July 2, 4 , 6, 8, 10.
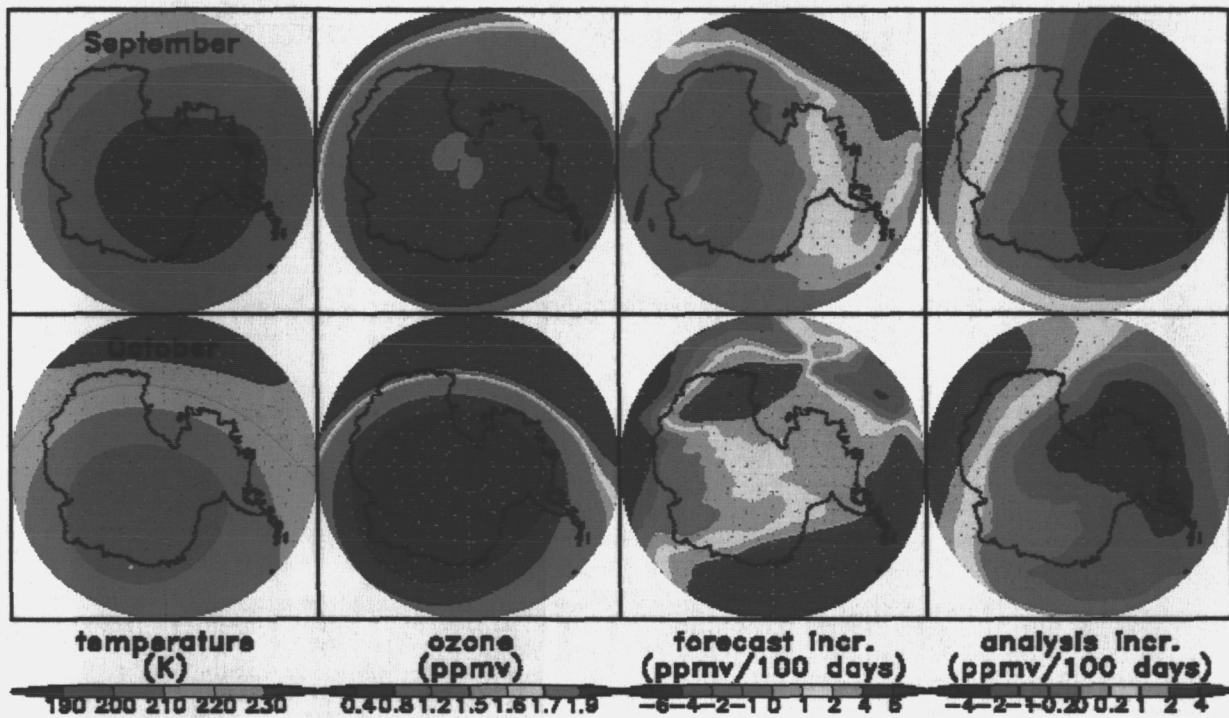
Figure 5. Mean fields at 70 hPa are shown for July (top row) to October 2003 (bottom row). The fields are temperature (first, leftmost column), ozone (second column), changes to the ozone due to forecast model (third column), analysis increments (fourth column). Southern polar stereographic maps are shown up to 60°S.
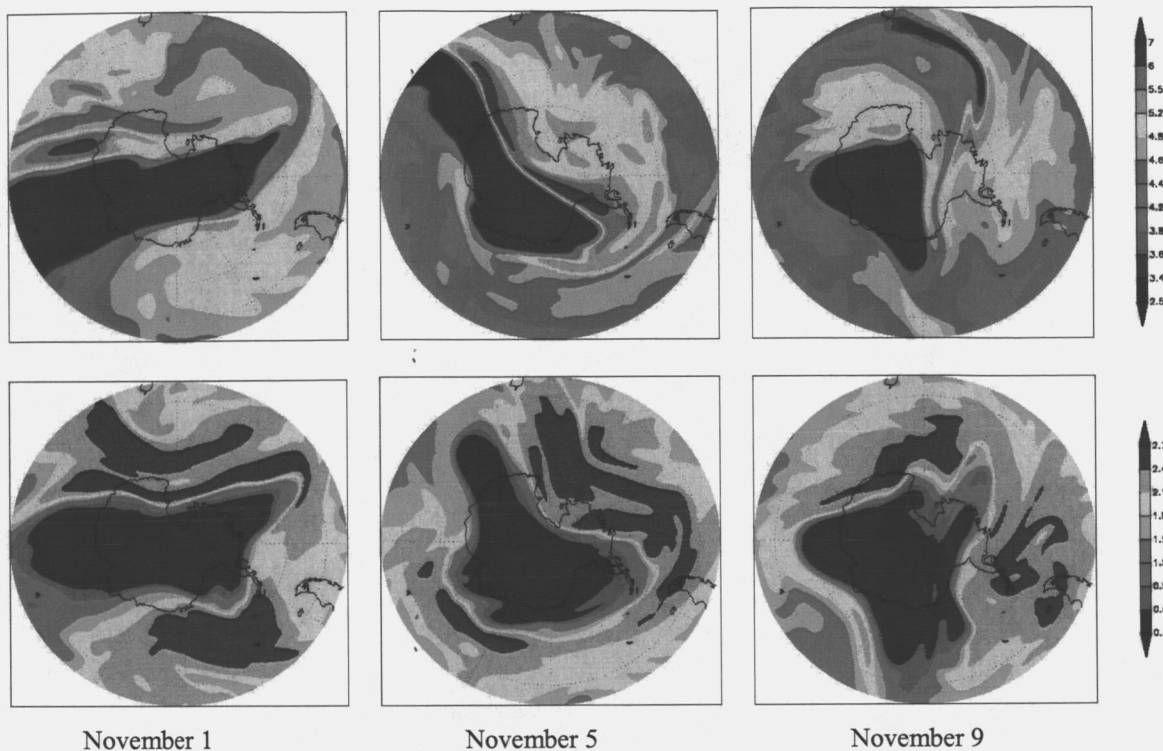
November 1   November 5   November 9

Figure 6. Ozone fields (ppmv) at 30 hPa (top row) and 70 hPa (bottom row) at 12 z on November 1 (left column), November 5 (center column), and November 9 (right column) are shown in the southern polar stereographic projection up to 45°S.
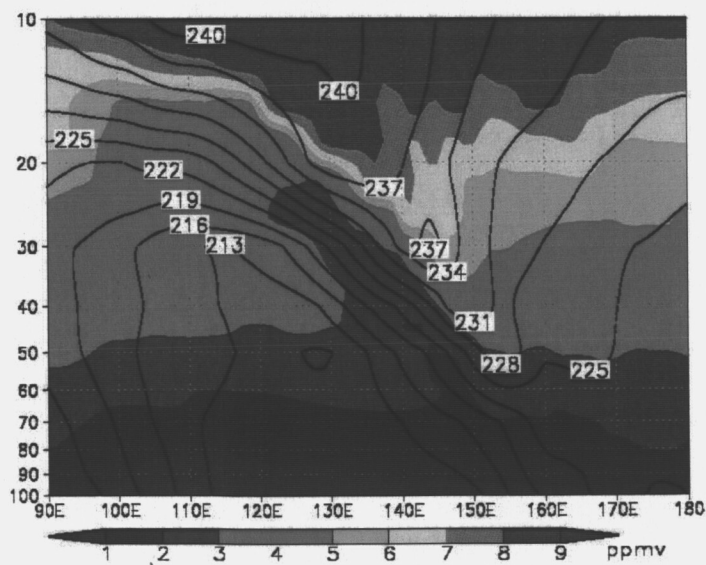
Figure 7. Longitude-pressure section at 50°S, between 90°E and the date line and 100-10 hPa, on November 5, 2003. The shading shows the analyzed ozone distribution (color scale with increments of 1 ppmv) and the contours show analyzed temperature (contour interval 3 K).
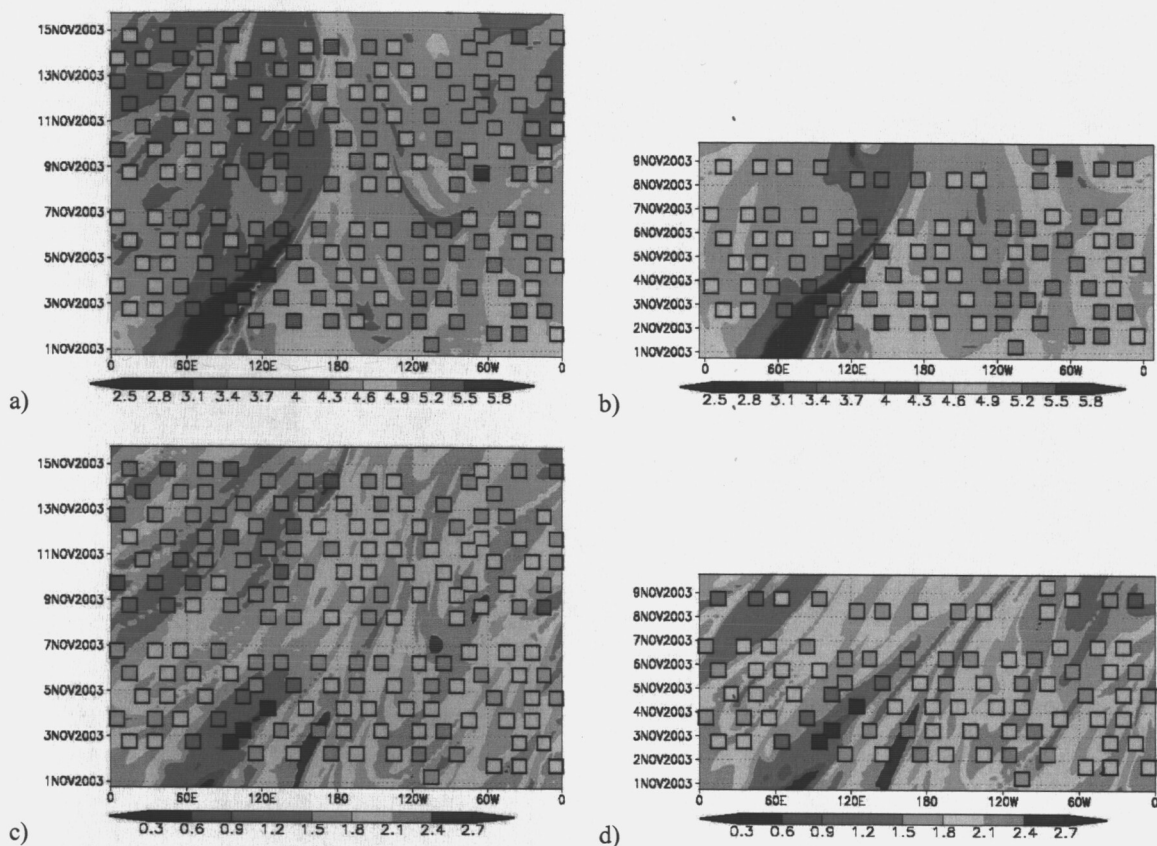
Figure 8. Ozone (ppmv) time series comparison for November 1-15 of SAGE III and analyses at 46°S at a) 30 hPa and c) 70 hPa. Comparison of SAGE III and ozone forecast started on October 30 at 18 z at b) 30 hPa and d) 70 hPa. Time range for forecast time series is November 1-9 (b and d). SAGE values are plotted in squares using the same color scale as in the underlying analysis or forecast fields.
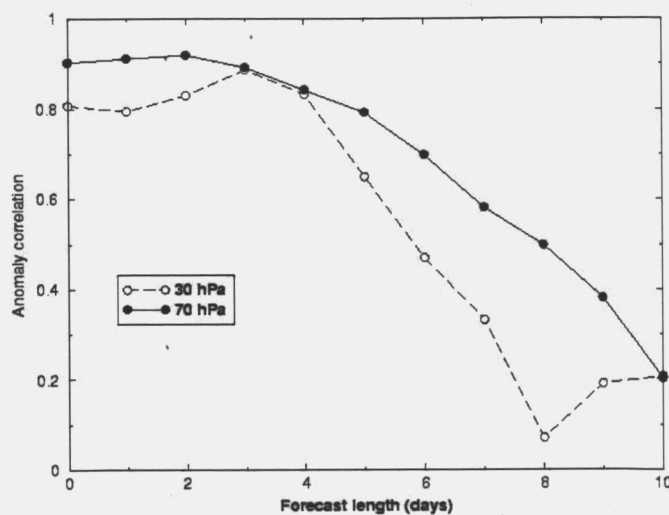
Figure 9. Anomaly correlations between SAGE III and collocated ozone forecasts as a function of forecast length at 70 hPa (solid) and 30 hPa (dashed).
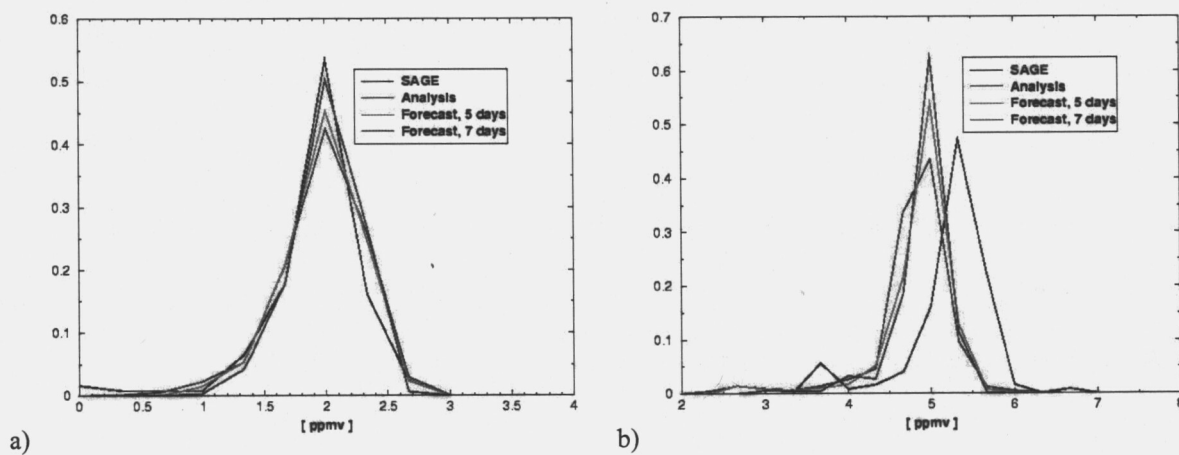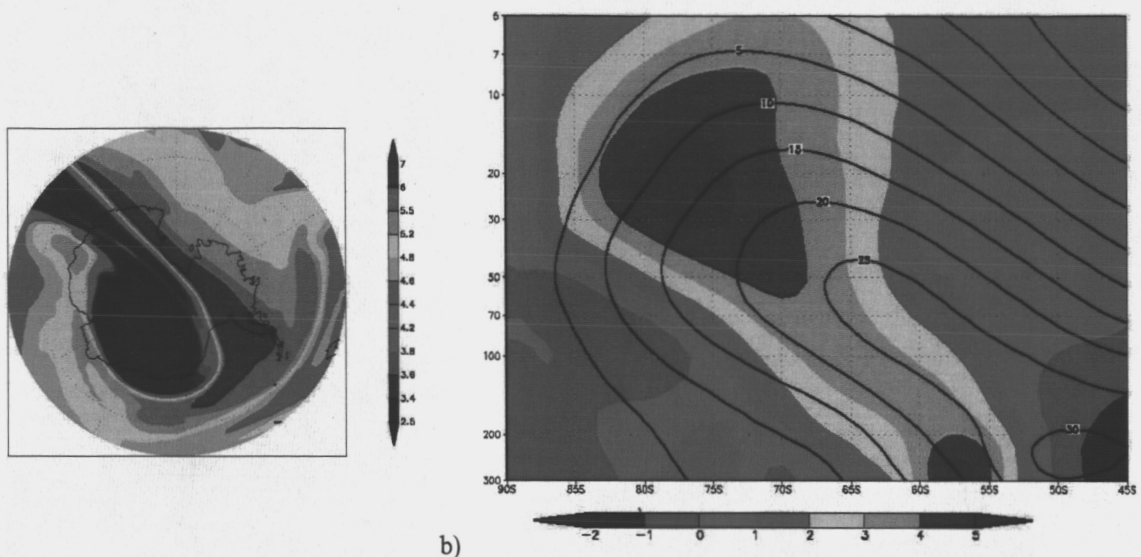

Figure 10. Normalized histograms of SAGE III ozone (black), analyses (red), five-day forecasts (green) and seven-day forecasts (blue) at 46°S for November 1-10 at a) 70 hPa and b) 30 hPa.

a)   b)

Figure 11. a) Five-day ozone forecast (ppmv) at 30 hPa for November 5 at 12z is shown (cf. analysis in Fig. 6, top row, center column). b) Average analysis zonal wind (m/s) for November 1-10 (contour) and the average difference between 5-day wind forecast and analysis (color) are shown for 90°S-45°S and 300-5hPa.